ORGANIC PROCESS RESEARCH & DEVELOPMENT
OPR&D

pubs.acs.org/OPRD

Article

A Structured Approach To Cope with Impurities during Industrial Crystallization Development

Stephanie J. Urwin, Guillaume Levilain, Ivan Marziano, Jeremy M. Merritt, Ian Houson, and Joop H. Ter Horst*

Cite This: *Org. Process Res. Dev.* 2020, 24, 1443−1456

Read Online

ACCESS | Metrics & More | Article Recommendations | Supporting Information

ABSTRACT: The perfect separation with optimal productivity, yield, and purity is very difficult to achieve. Despite its high selectivity, in crystallization unwanted impurities routinely contaminate a crystallization product. Awareness of the mechanism by which the impurity incorporates is key to understanding how to achieve crystals of higher purity. Here, we present a general workflow which can rapidly identify the mechanism of impurity incorporation responsible for poor impurity rejection during a crystallization. A series of four general experiments using standard laboratory instrumentation is required for successful discrimination between incorporation mechanisms. The workflow is demonstrated using four examples of active pharmaceutical ingredients contaminated with structurally related organic impurities. Application of this workflow allows a targeted problem-solving approach to the management of impurities during industrial crystallization development, while also decreasing resources expended on process development.

KEYWORDS: *impurity rejection, crystallization, product purity, phase diagrams, workflows*

INTRODUCTION

Crystallization is a highly selective separation and purification technique used across the pharmaceutical industry.[1] The quality of a crystallization product is defined by four principal attributes: chemical purity, polymorphic form, particle size, and crystal morphology. Analyzing chemical purity is therefore of critical importance during development of a crystallization process. Ideally after crystallization, the resulting solid particulate product is composed of one single target compound with all other chemical entities remaining in the liquid phase for disposal. In reality, the majority of the impurity is rejected by the growing crystals, but some impurity compromises the final product purity. Ranitidine is an example showing the impact of an impure product: In 2019, the US Food and Drug Administration recalled ranitidine, a common heartburn medication, due to unacceptable levels of the known carcinogen *N*-nitrosodimethylamine.[2] Samples were found to contain up to 9 times (0.86 μg) the recommend safe daily ingestion level (0.096 μg) in a single 300 mg ranitidine dose.[3]

It is essential to remove residual impurity compounds to below a threshold concentration value, as they could have unwanted, even detrimental, biological effects above it.[4] Coping with too high concentrations of impurities in crystalline products can be challenging,[5] and impurity rejection is typically tackled on a case by case basis.[6] Industry requires a targeted approach, the methodology of which can be transferred to any novel system. We present here a general workflow to identify the mechanism of impurity incorporation responsible for poor impurity rejection during crystallization through four problem solving stages. Once the impurity incorporation mechanism is identified, specific targeted changes can be made to the process design in order to reduce the final impurity concentration below its set specifications.

IMPURITIES IN CRYSTALLIZATION

An array of mechanisms of impurity incorporation into a solid particular product exist.[6−8] From literature, we identified five principal methods of product contamination during crystallization (Figure 1); agglomeration, surface deposition, inclusions, cocrystal formation, and solid solution formation. These methods are principally based on the location of the impurity within the crystallization product, and may result from several different mechanisms.

Agglomerates. When particles aggregate during a crystallization to form larger agglomerates, pockets of impurity-rich mother liquor can become trapped between the intergrown particles, which then results in a substantial impurity content of the product after secondary processing.[9] General methods to avoid agglomeration include lowering the degree of supersaturation and controlling the agitation rate,[10] however more specific methods have been developed for extreme cases. Paracetamol is known to agglomerate when crystallized from nonpolar solvents.[11] This unwanted process can be suppressed by the application of ultrasound[12] and was found to also increase the overall impurity purge of the

Received: April 7, 2020
Published: July 6, 2020

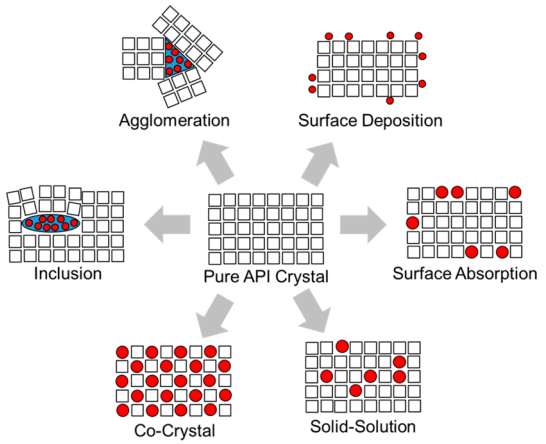

Figure 1. Schematic representation of various methods of low-level impurity incorporation during crystallization.

process.[13] In the case of agglomeration-prone piroxicam monohydrate, the addition of temperature cycling to a seeded antisolvent crystallization resulted in larger, well separated crystals.[14]

Surface Deposition. Impurities can be present on the crystal surface of the final product particles. This can result from residual mother liquor that has not been adequately washed away in the solid−liquid separation. Additionally, where impurities have a high affinity for the crystal surface, adsorption onto the crystal surface can reduce crystal purity.[15−17] The addition of a methanol wash after the filtration of β-methyl-tetra-*O*-acetyl-D-glucopyranuronate resulted in the removal of trace residues of the α-enantiomer present in unwashed crystals.[18] In the crystallization of bisphenol A, a different problem solving approach was taken when the adhesion of mother liquor was found for the source of unwanted impurity molecules: Modification of crystallization conditions to increase overall particle size and remove small, fine particulates allowed for improved filtration of the product, resulting in an effective removal of the mother liquor and with it an increase in the purity of the crystals.[6]

Inclusions. Macroscale impurity incorporation can also occur through the inclusion of impurity-rich mother liquor within the growing crystal. Growth-induced inclusions, typically due to rapid crystal growth rates, are a function of surface kinetics. Interactions between the API (active pharmaceutical ingredient) crystal face and surrounding solvent molecules can also be responsible for inclusion formation. In the case of thiourea, crystallization from polar solvents leads to increased macroscale, growth-induced inclusions through electrostatic interactions with the polar growing surface.[19]

Due to stirrer-particle and interparticle collisions, crystal attrition can occur in suspensions with high energy agitation, which leads to attrition-induced inclusions in the colliding particles, usually only above a certain size.[20] Inclusions resulting from crystal attrition can lead to compromised product purity. It is well documented that impurity incorporation is a function of vessel stirring rate.[21−24] When crystallizing paracetamol from water in a 500 mL round-bottom flask with *p*-acetoxyacetanilide present, increasing the stirring speed from 200 to 320 rpm increases product purity; however, increasing further to 400 rpm leads to higher impurity incorporation.[22]

Typically, only a very small amount (<5 w%) of solvent can be occluded,[21] but this can have a significant effect on the crystal properties. Rigorous drying processes might remove occluded solvent with a high volatility; however, nonvolatile impurity compounds remain captured kinetically within the crystal. The probability of solvent encapsulation occurring increases with crystal growth rate and final particle size and results in particles with significant surface defects.[21]

Cocrystals. Novel cocrystal structures can result from noncovalent interactions between multiple species, resulting in regular incorporation of both compounds into the crystal lattice. Formation of cocrystals of APIs with specifically chosen coformers is a proven method to improve product attributes and/or therapeutic effect, for which several reviews are available.[25−27] However, sometimes the product and an impurity form an insoluble cocrystal. For instance, Melamine and its hydrolysis product cyanuric acid form a toxic 1:1 cocrystal which is virtually insoluble,[28] making the separation of the two component compounds by crystallization challenging, as the eutectic point in the ternary phase diagram is very close to the pure component axis. Consequently, a small amount of cocrystal will concomitantly form with one of the pure component products.

Solid Solutions. A (partial) solid solution can form where there are substantial similarities between crystal structures and packing. Carbamazepine is a polymorphic API with a well-studied solid-solution landscape. For example, carbamazepine form V and its hydrogenated analogue share an unusual catameric structure, and together they form solid solution crystals.[29] In the case of metastable carbamazepine form II, the insertion of small amounts of high boiling solvents into lattice voids provides significant thermal stabilization.[30,31] As such solid-solution formation depends on isomorphic crystal lattice packing, it is polymorph specific. Despite the existence of multiple polymorphs, mefenamic acid and its des-methyl chlorinated analogue tolfenamic acid only form a solid solution between the respective I/VI polymorphic pairing.[32]

Such solid-state miscibility, whereby the impurity is thermodynamically substituted irregularly into the crystal lattice due to structurally similarity, is characterized by a distribution of the impurity throughout bulk crystal material.[6,33] The even distribution of the impurity paracetamol in phenacetin crystals was shown by stepwise dissolution of large single crystals, which is hypothesized to be due to formation of a solid solution.[33] Ineffective purification of phenanthrene in the presence of impurity 9,10-dihydroanthracene by crystallization due to partial solid-solution formation between the components was demonstrated by analysis of the binary phase diagrams.[34] Partial miscibility between a pair of α- and β-epimers (2.6% for α in β and 4.4% for the reverse) was revealed by construction of binary phase diagrams and subsequent Tammann triangle plots.[35] When considering the purity required for crystalline API compounds, such low levels of miscibility could pose an issue to the purification process. When considering the extent of impurity incorporation is a function of crystallization driving force, i.e. degree of supersaturation and growth rate, the existence of solid-state miscibility will unavoidably increase the amount of product contamination after crystallization.

With consideration to the methods of impurity incorporation discussed, we undertook the development of a structured approach to identify which of the mechanisms is

https://dx.doi.org/10.1021/acs.oprd.0c00166
Org. Process Res. Dev. 2020, 24, 1443−1456

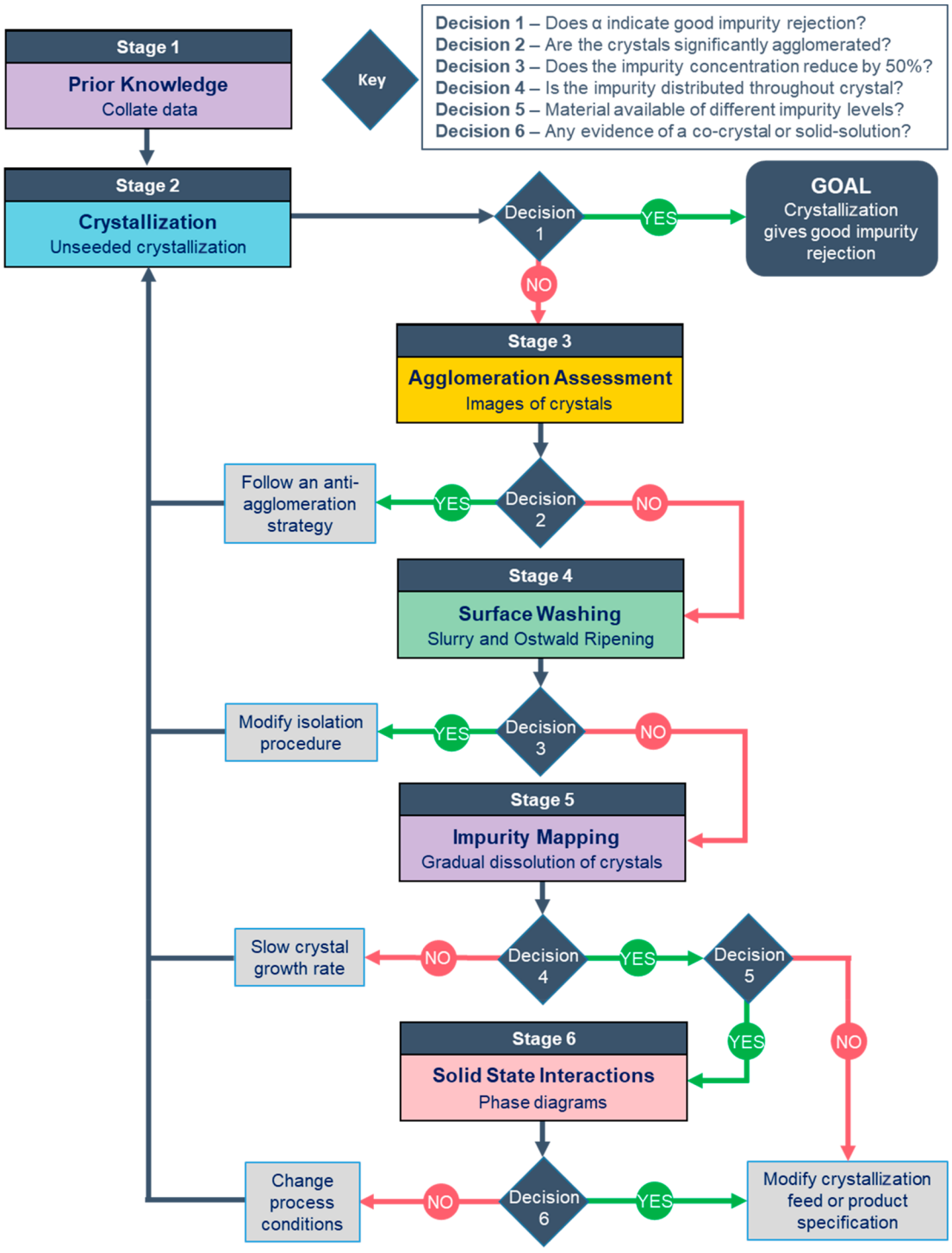

Figure 2. Impurity rejection workflow.

responsible for compromised product purity which could generally be applied to any crystallization process.

Impurity Rejection Workflow. Figure 2 shows the developed Impurity Rejection Workflow, considering the identified mechanisms of impurity incorporation. The aim of the novel workflow is to give a structured experimental approach to identify the mechanism of impurity incorporation, and the underlying knowledge and experimental techniques used within the workflow can be found in literature. The outcomes of the experimental stages are scrutinized by six decisions, from which the identification of the mechanism subsequently allows for a targeted mission to improve impurity rejection for a crystalline product within specifications. The exact definition of sufficient impurity rejection will depend on the product to which it is being applied. During the workflow, the crystallization behavior and product quality of the API are investigated, and if the product impurity concentration is higher than required, the material is subjected to a series of experiments which become more practically laborious and material intensive as the steps progress. Each subsequent stage consists of simplified experimental guides to rapidly and

https://dx.doi.org/10.1021/acs.oprd.0c00166
Org. Process Res. Dev. 2020, 24, 1443−1456

efficiently identify or exclude a specific impurity incorporation mechanism.

Stage 1: Baseline Knowledge. The first stage of the workflow involves the collation of baseline knowledge required to carry out the subsequent five stages. Specific data items are listed in Table 1. This information is likely already available to the user, or it may require the collection of extra physical data or simulation results.

Table 1. List of Prior Knowledge Required to Complete the Workflow

	Data Item	Priority	Method
1	Crystallization product specification	Essential	—
2	Development of crystallization procedure	Essential	Workflow[36]
3	Physical data of API, including T_m and H_{fus}	Essential	Literature search or experimental measurement
4	Physical data of impurities, including T_m and H_{fus}	Desirable	Literature search or experimental measurement
5	Analytical method calibration for API and impurities	Essential	e.g. HPLC

The first essential data item is product specification. Before undertaking a crystallization, the user must know what product specifications they are pursuing, including, but not limited to, the chemical purity. In the absence of such specifications for an API compound, current ICH guidelines require that unidentified impurities must not be present in amounts greater than 0.1% for a drug substance, and concentrations of genotoxic impurities, i.e. compounds which interact with biological processes or DNA, must be "as low as reasonably practical".[37]

The target polymorph should also be included in the product specification. It was noted that the presence of impurities has been reported to induce polymorphic transformations during crystallization which can directly affect impurity rejection behavior;[38−40] however, this was classified as out of scope during this work. It is assumed going forward that the crystallization leads to the isolation of the specified product polymorph.

As the impurity rejection workflow does not include any steps which aid the design of a crystallization, the second essential data item listed in Table 1 is a standard crystallization procedure, usually following from a crystallization design workflow. This procedure encompasses data such as the temperature-dependent solubility of the API, and perhaps of impurities, in the relevant solvents as well as a product isolation procedure. This impurity rejection workflow was formulated to complement crystallization design workflows, such as the comprehensive continuous seeded crystallization workflow recently reported.[36]

Knowledge of the physical properties of the API decides what process conditions are practical. Specifically listed in Table 1 are the melting point T_m and enthalpy of fusion H_{fus}, as they are required for the thermal measurements conducted in Stage 6. Similar information for the impurity material in the system would be useful although this may not be feasible in some applied industrial development situations, and the workflow can be applied without knowledge of the impurity identity. Finally, analytical methods must be available to measure crystal purity within the limits specified.[41] The most common way to do this is using HPLC, as it offers accurate concentration measurements for very small quantities.

Stage 2: Crystallization and Decision 1. The objective of Stage 2 is to crystallize the API in the presence of controlled amounts of impurities, and to determine whether these impurities have been sufficiently rejected. The isolated product material is then used for the experiments in the subsequent Stages 3−5. Although the specific method of crystallization (cooling, antisolvent, evaporative) is not crucial to the application of the workflow, the procedure should give reproducible product quality, yield, and purity. Therefore, a well-thought through crystallization process should be used that considers process conditions such as cooling profile or addition rate in respect to nucleation and growth behavior during the crystallization.[10]

There are various reported ways to determine the extent of impurity rejection during crystallization.[42−44] Here, we use the selectivity (α) of the process. After completion of the crystallization process, the partition of each component c across the two phases is calculated as the experimental distribution coefficient K using eq 1. X_s^c is the mole fraction of the component in the solid phase after crystallization, and X_l^c is the corresponding mole fraction in the liquid phase.

$$K_c = \frac{X_s^c}{X_l^c} \tag{1}$$

The effectiveness of impurity removal during this crystallization is subsequently determined by the selectivity α (eq 2).

$$\alpha = \frac{K_i}{K_A} \tag{2}$$

The ratio of the distribution coefficient K_i, of the impurity, and the distribution coefficient K_A, of the API, will usually give an α value between 0 and 1. An α value of 0 indicates the impurity has been completely rejected by the crystals during the process, where a value of 1 means that the crystalline material has equal preference to take up impurity and solute. In general, due to the limitations of fitting a foreign molecule in a lattice, for crystal products the selectivity is quite close to zero, leading to low impurity concentrations in the final product. Where a solid solution or cocrystal has formed, α will be higher. Decision 1 asks the user whether α indicates good impurity rejection, and the criteria for this can vary depending on the specific system. Using α also provides a method of comparing crystallization outcomes of different APIs, impurities, and/or solvents.

The maximum allowed value for α is dictated by the purity required and the concentration of the impurity in the crystallization feed, which is summarized in Figure 3. For example, to achieve a product purity of 99.0 mol % from a feed containing 10 mol % impurity ($X_{IMP} = 0.10$), the process, $\alpha \leq 0.012$. If the specification is less stringent, and 95 mol % was the required purity, $\alpha \leq 0.122$ for the same crystallization. In practicality, the value of α should be as low as possible, and if there are no purity specifications set, we recommend aiming for $\alpha < 0.05$. As an example, we can consider ranitidine contaminated with *N*-nitrosodimethylamine. A daily dose of up to 600 mg of ranitidine can be prescribed. When considering the recommended safe daily ingestion level of known contaminant *N*-nitrosodimethylamine is 0.096 μg per day, and assuming *N*-nitrosodimethylamine is removed by crystallization, ranitidine API product cannot contain more than 0.0001 mol % of the impurity. If this represents a 90% removal

https://dx.doi.org/10.1021/acs.oprd.0c00166
Org. Process Res. Dev. 2020, 24, 1443−1456

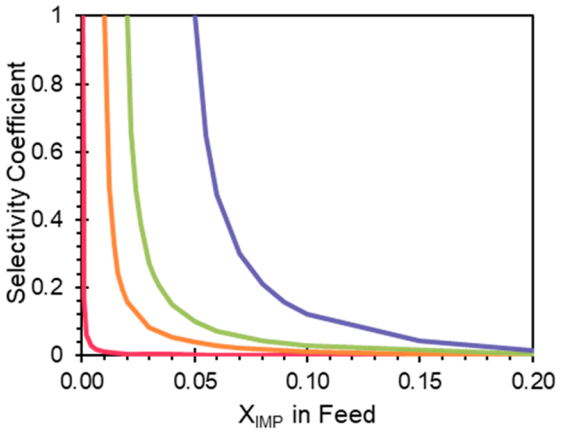

Figure 3. Product purity required affect the maximum acceptable value for selectivity coefficient. (Red) 99.5 mol % product purity; (orange) 99.0 mol % product purity; (green) 98.0 mol % product purity; (blue) 95.0 mol % product purity; all assuming 80% product yield from the crystallization process.

of the impurity and a reasonable crystallization yield of 75%, subsequently $\alpha = 0.038$ (see Table S1).

Stage 3: Agglomeration Assessment and Decision 2. It is likely that Stages 1 and 2 already in some way form part of the user's crystallization design workflow,[36] and thus here do not present any extra experimental undertaking. If the impurity rejection obtained through this route is not sufficient, it is then that this workflow can be followed to identify the mechanism of impurity incorporation into the product. In Stage 3, the isolated crystals are examined for agglomerates. In general, agglomerates are unwanted (with notable exceptions, for example spherical agglomeration[45]), and here they are unwelcome due to the trapping of impurity-rich mother liquor inclusions in the bridge between agglomerated crystalline particles.[9]

Decision 2 asks the user if the crystals are significantly agglomerated. Free-flowing particles would give a negative answer to this question: the impurity incorporation for the system follows another mechanism, and the user moves to Stage 4. Should microscopy confirm the presence of agglomerated crystals, leading to a positive outcome for Decision 2, the workflow suggests the user return to the crystallization stage and implement an antiagglomeration strategy. Altering the crystallization design, for example selection of a different solvent, performing crystallization under a reduced supersaturation, or changing fluid dynamic conditions, may be required in this case.[14,36] A successful antiagglomeration strategy will likely reduce the impurity incorporation, as impurity-rich mother liquor phase cannot be trapped between crystallized particles. Identifying agglomeration is achieved by imaging the isolated particles. In this work we have used optical microscopy, as it is an efficient, nondestructive technique requiring little material; however, *in situ* methods of imaging particles, for example the use of a Particle Vision and Measurement (PVM) probe, would also provide insight into whether agglomeration has occurred during the crystallization process.

Stage 4: Surface Washing and Decision 3. Should agglomeration not be the mechanism of impurity incorporation, the next step of the workflow investigates the extent of impurity deposition and/or adsorption on the surface of crystals. This occurs in the later stages of crystallization, and unlike incorporation, the impurity does not substitute into the crystal lattice. This results in high concentrations of impurities at the surface of the crystal in the product, hence, requiring the same mitigation strategy.

The concentration of impurities at the crystal surface can be investigated through slurry experiments. Suspension and low energy agitation of a product sample in a saturated impurity-free API solution thoroughly washes the crystal surface to remove impurities deposited by mother liquor and allows the surface layers to further reject impurity molecules through constant interaction at the crystal−solution interface. Analysis of solid phase purity after this slurry process would show a significant increase in purity (>50% of the impurity is removed) if the impurity molecules are located solely in the surface layers of the crystals. Impurity rejection in these cases can be enhanced by fine-tuning the filtration and washing steps after the crystallization.[7] If the impurity concentration in the solid phase remains high after this process, impurity incorporation is not the result of surface adsorption or deposition and the user proceeds to Stage 5.

Stage 5: Impurity Mapping and Decision 4. Stage 5 extends the knowledge gained in the surface experiments. By creating a distribution map of the impurity throughout the bulk crystal, it will confirm whether the impurity has been incorporated throughout the growth of the crystals. In an experimental method modified from recent literature,[46−48] portions of pure solvent are added to a suspension of crystal product in saturated API solution, to slowly dissolve the contaminated crystals. The concentration change of impurity in the liquid phase upon dissolution gives information on the distribution of impurity throughout the crystal bulk, which is then considered in Decision 4.

There are various outcomes of the impurity mapping measurement, with some examples depicted in Figure 4. If

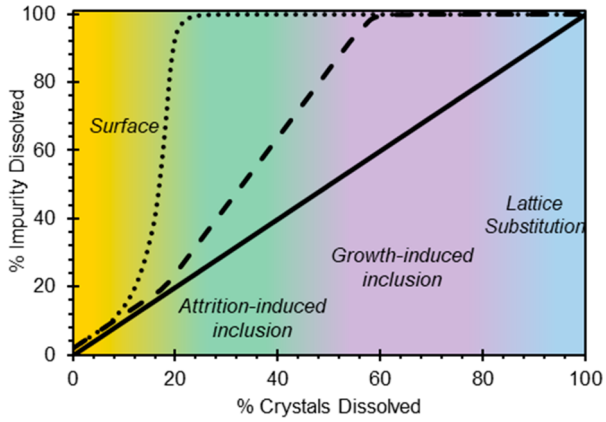

Figure 4. Examples of possible impurity distribution maps. The colored zone where the impurity reaches 100% dissolution gives an indication of the contamination mechanism. (···) Impurity distributed in the outer layers of the crystal. (- - -) Impurity present due inclusions. (—) Impurity regularly distributed through the crystal bulk.

the impurity molecules are exclusively present in the outer layers of the crystals, the impurity concentration c_i will sharply increase in the first solvent addition steps and then remain constant (Figure 4, surface). When accompanied by a decrease in impurity content during slurry experiments completed in Stage 4, this result would give further support to conclude

https://dx.doi.org/10.1021/acs.oprd.0c00166
Org. Process Res. Dev. 2020, 24, 1443−1456

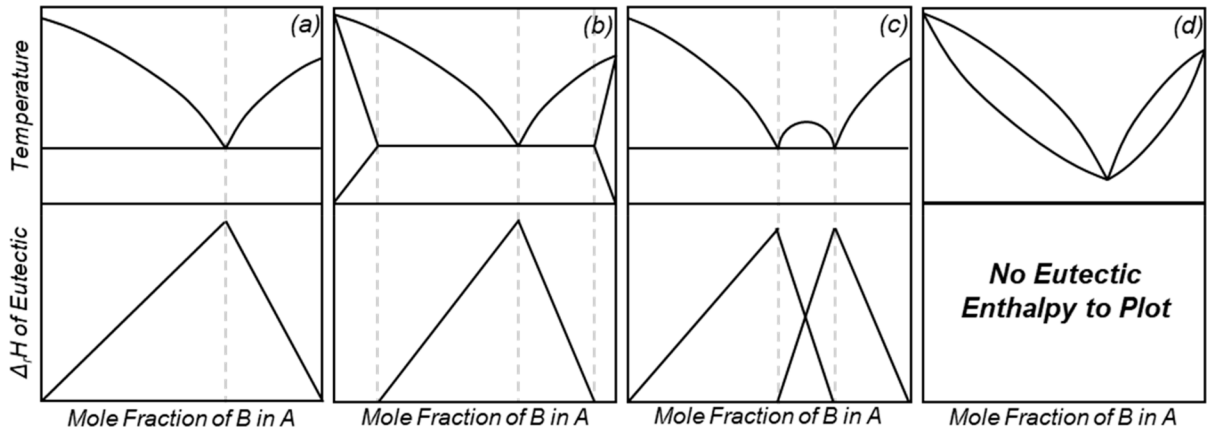

Figure 5. Types of binary phase diagram (top) and accompanying Tammann triangle plots (bottom).[51] (a) Simple eutectic with no solid solution, (b) partial solid solution, (c) cocrystal, and (d) full solid solution.

surface deposition/absorption is responsible for contamination, and the same mitigation strategy as suggested for Stage 4 should be used.

A more steady increase in impurity concentration c_i which reaches full impurity dissolution during the middle stages of the bulk crystal dissolution would indicate significant growth-induced or attrition-induced inclusions (Figure 4, inclusions). The presence of inclusions can be investigated further using imaging techniques such as high resolution microscopy.[20,49,50] The distribution of macroscopic solvent inclusions in a crystal is determined by its growth and collision history, which in turn are strongly related to the process conditions during crystallization. While it may be difficult to pinpoint to a responsible inclusion formation mechanism from the impurity mapping experiments, the dissolution trends allow the user to prioritize subsequent experimental approaches to do so. Strategies to alleviate solvent inclusions include reducing the rate at which the crystallizing solution desupersaturates[21] and modifying the hydrodynamics to reduce stirrer−particle and interparticle collisions.[22]

Confirming surface deposition or inclusions, i.e. where the % impurity dissolved reaches 100% when 20−80% of the bulk crystal has dissolved, would give a negative outcome to Decision 4, as the impurity is present within the bulk crystals. In the case of growth induced inclusions, growth kinetics can have a significant negative impact on crystal purity.[16,50] The suggested mitigation strategy is to modify the process conditions to give a different growth regime, for example changing the supersaturation at which nucleation occurs. Where the impurity is distributed uniformly throughout the bulk crystal, it is likely that incorporation has occurred during the crystal growth (Figure 4, lattice substitution).[47] This would give a positive outcome to Decision 4, and the user proceeds to Decision 5.

Decision 5, Stage 6: Solid State Interactions and Decision 6. The objective of Stage 6 is to identify any (partial) solid solution formation between the API and impurity, as such behavior would impede the purification efficiency of a crystallization. Binary phase diagrams are an effective way to determine whether two solids are miscible in the solid state. In a simple eutectic system, the two liquidus curves intersect at the eutectic point, and in the absence of any solid miscibility results in four regions in the phase diagram (Figure 5a). The presence of partial solid miscibility to the phase diagram introduces tie-lines indicating areas of solid solution formation (Figure 5b). In a fully miscible system, such as a solid solution, this eutectic point is absent as the API and impurity together form crystalline material, competing for the same lattice positions during growth (Figure 5d). Any formation of true cocrystals between the API and impurity, which would also hinder purification, will also be evident from the binary phase diagram (Figure 5c). These situations are confirmed by the accompanying Tammann triangle constructed from the same data required for the binary phase diagram.[51] The intersection of two (or more, Figure 5c) linear relationships defines the true eutectic composition, and the corresponding x-axis intercepts denote any partial solid miscibility. This type of thermodynamic analysis has been applied to pharmaceutical systems with multicomponent formulations, where solid state interactions are essential.[52,53]

As building phase diagrams is particularly material intensive, preceding Stage 6, Decision 5 asks the user to consider whether sufficient material is available to complete the solid-state behavior experiments. This is a simple question, but it may not be straightforward to answer; the absolute amount of material required will heavily depend on the detail required. In many applications, it is unlikely that pure impurity is available for experimentation. However, construction of the binary phase diagram only up to 10% impurity concentration will likely not yield a different conclusion to a full phase diagram. Using the methods described here, of combining dilute stock solutions to give a range of accurate mole fractions after evaporation, enough information to construct a useful partial Tammann triangle can be achieved with just a few milligrams of pure impurity, or alternatively mixtures of impure and purified API from synthetic streams can be used to vary impurity concentration. Where the conditions of Decision 5 are still not satisfied, a negative outcome to Decision 5 leads to the suggestion of changing the chemistry so that this impurity is no longer present in crude product streams in significant concentrations. This is justified, as although the impurity mechanism has not been identified thus far, the thermodynamic impurity is posing a serious challenge which needs to be mitigated.

Differential scanning calorimetry (DSC) analysis of samples with different molar API-impurity ratios allows the experimental binary phase diagram to be plotted. Inspection of this phase diagram will indicate whether, for example, the mixtures form a complete solid solution. Where eutectic signals are identified in the DSC analyses, a plot of the signal enthalpy

https://dx.doi.org/10.1021/acs.oprd.0c00166
Org. Process Res. Dev. 2020, 24, 1443−1456

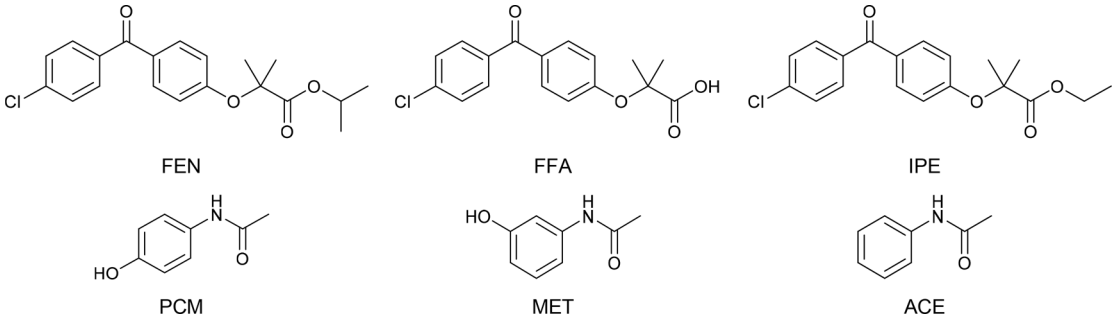

Figure 6. Structures of APIs and impurities used to demonstrate the workflow; fenofibrate (FEN), fenofibric acid (FFA), fenofibrate impurity E (IPE), paracetamol (PCM), metacetamol (MET), and acetanilide (ACE).

Table 2. Summary of Example Crystallizations Discussed[a]

	API	Impurity	S	${}^{f}c_i$ (mol %)	${}^{s}c_i$ (mol %)	K_A	K_i	α
1	FEN	FFA	3.0	7.64	1.63	1.352	0.060	0.044
2	FEN	IPE	3.0	9.48	6.43	1.091	0.453	0.415
3	PCM	ACE	2.1	5.01	0.80	1.090	0.069	0.063
4	PCM	MET	2.1	4.02	2.51	1.075	0.270	0.251

[a] S = relative supersaturation ratio; ${}^{f}c_i$ = concentration of impurity in crystallization feed; ${}^{s}c_i$ = concentration of impurity in the crystal product; K_A = experimental distribution coefficient of API; K_i = experimental distribution coefficient of the impurity; α = selectivity coefficient of crystallization.

versus the impurity mole fraction X_i gives a Tammann triangle plot.[51] The x-axis intercept of the linear relationship between X_i and the enthalpy of the eutectic signals corresponds to the solid−solid miscibility gap between the API and impurity; i.e., an x-axis intercept of $X_i = 0.05$ indicates a partial miscibility of approximately 5% of impurity with the API lattice.

After inspection of the phase diagram and Tammann triangle plot, Decision 6 asks the user if any solid state interactions have been identified. Each phase diagram in Figure 5 requires a different mitigation strategy. Some strategies go beyond adaption of crystallization design.[40] A partial solid solution concentration beyond the upper limit impurity concentration for instance limits the achievable crystallization selectivity. The impurity rejection issues will have to be mitigated using other separation technologies or changes to process chemistry.

Summary of Workflow. The Impurity Rejection Workflow depicted in Figure 2 offers a structured approach to overcoming compromised product purity. After compiling the background knowledge and initial crystallization, scrutinizing the chemical purity determines whether effective impurity rejection has been achieved. The impurity concentration is not acceptable, the extent of agglomeration is determined, which indicates if impurity-rich mother liquor has become trapped. If this is not the cause, the crystals are examined for deposition and/or absorption of impurities onto the crystal surface. To inspect further, the distribution of the impurity can be mapped using stepwise dissolution techniques. Finally, the phase diagram of the binary system is determined to quantify any solid miscibility of structure, which would likely hinder purification. The resulting knowledge gained from using this workflow would help the user identify which impurity mitigation strategy would most likely improve the purity of the crystallization product in a resource efficient manner.

Case Studies. To demonstrate use of the impurity rejection workflow, four case studies are presented. Each system constitutes a target API to be crystallized and one structurally related impurity. It is noted that the workflow can be applied to systems where multiple impurities are present in varying amounts, for example a synthetic stream output, with little change to the experimental strategy.

Crystallizations of paracetamol (PCM) and fenofibrate (FEN) were examined with the added structurally related organic impurities acetanilide (ACE), metacetamol (MET), fenofibric acid (FFA), or fenofibrate impurity E (IPE) (Figure 6). These are well-studied model compounds, and as such the collation of baseline knowledge for Stage 1 of the workflow was almost solely completed through literature searches. The exception to this was the H_{fus} value for IPE, which was experimentally measured using DSC (Figure S1). The results of Stage 1 for all systems can be found in the Supporting Information.

All cooling crystallizations for Stage 2 were carried out under supersaturation-controlled nucleation; the specific temperature-transmission profiles can be found in Figures S4−S7. Both paracetamol and fenofibrate are polymorphic APIs, and for all crystallizations the isolation of the targeted stable form I polymorph was confirmed by X-ray powder diffraction (Figures S8 and S9). Reasonable product recovery was observed in all cases, as calculated using the literature solubility values collated in Stage 1 (Figure S2). Each crystallization purified the solid phase to some degree although the extent of impurity rejection varies greatly across this short series.

Example 1: Fenofibrate−Fenofibric Acid. Fenofibrate is a common lipid lowering medication, and the active metabolite, Fenofibric acid, forms via ester cleavage. The required fenofibrate purity in this work is 98.0 mol %, and the crystallization conditions chosen give a maximum product yield of 82.6%. This leads to a selectivity coefficient limit of 0.045.

An initial concentration of 7.64 mol % FFA is decreased to 1.63 mol % in the isolated solid phase (Table 2, entry 1), which gives an experimental selectivity coefficient α_{FFA} of 0.044. This low value gives a positive outcome for Decision 1, and the goal of a crystallization with good impurity rejection is reached.

Example 2: Fenofibrate−Impurity E. Another impurity present in fenofibrate crystallization feeds is an analogous ethyl

https://dx.doi.org/10.1021/acs.oprd.0c00166
Org. Process Res. Dev. 2020, 24, 1443−1456

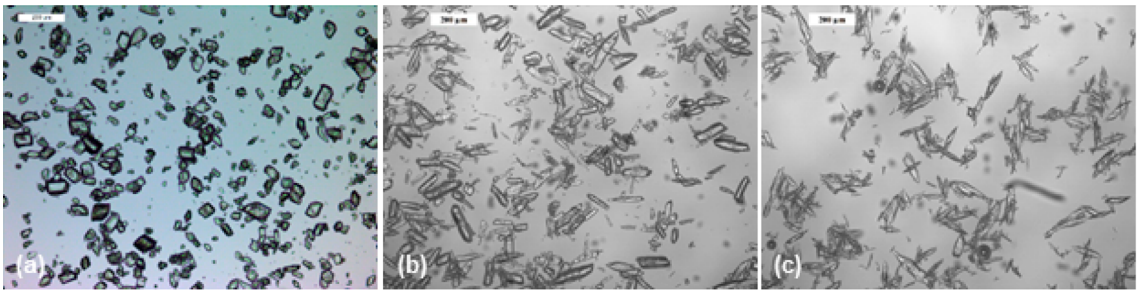

Figure 7. Optical microscopy images of API crystals containing significant impurity concentrations. (a) Fenofibrate contaminated with 6.43 mol % impurity E. (b) Paracetamol contaminated with 0.80 mol % acetanilide. (c) Paracetamol contaminated with 2.51 mol % metacetamol.

ester, ethyl 2-[4-(4-chlorobenzoyl)phenoxy]-2-methylpropanoate, named in the European Pharmacopeia as Impurity E. A higher purity restriction of 99.8 mol % gives a lower α limit of 0.002.

In contrast with FFA, IPE significantly contaminates crystalline FEN after the same crystallization and isolation procedures (Table 2, entry 2). An initial concentration of 9.48 mol % gave an impurity concentration c_{IPE} of 6.43 mol % in isolated FEN crystals. The corresponding selectivity coefficient α_{IPE} 0.415 indicates poor impurity rejection, and the material is taken to Stage 3 of the workflow. Optical microscopy images of the isolated material show well-separated crystals with a prismatic morphology (see Figure 7a). As no agglomeration is observed, Decision 2 requires the material is taken forward to Stage 4. Surface washing did not significantly reduce the impurity contamination of IPE in FEN (Table 3, entry 1). A

Table 3. Summary of Surface Washing Reslurry Experiments[a]

	API	Impurity	$^{s}c_i$ (mol %)	$^{sw}c_i$ (mol %)
1	FEN	IPE	6.43	4.25
2	PCM	ACE	0.80	0.27
3	PCM	MET	2.51	1.17

[a] $^{as}c_i$ = concentration of impurity in the crystal product; $^{sw}c_i$ = concentration of impurity in the slurry product.

reduction of c_{IPE} from 6.43 mol % to 4.25 mol % indicates that a significant amount of the impurity is not dissolved into the solution phase during the reslurry process, and therefore the bulk crystal was examined in Stage 5.

Gradual dissolution of a sample of the contaminated FEN crystals confirms that the impurity is dispersed within the bulk crystal; however, the distribution is not uniform. As shown in Figure 8, the IPE HPLC peak area% in the solution phase was constant after the first solvent portion was added and then increases sharply after the second. Smaller increases were observed in subsequent steps, followed by a plateau after approximately 60% of the suspended material has dissolved. This latter observation suggests that, during the crystallization, pure FEN was nucleated and began to grow, but part way through the growth phase, IPE began substitution into the growing crystal lattice. This indicates either thermodynamic incorporation or significant attrition inclusions are responsible for the compromised product purity. To investigate this nonuniform dissolution further, this case study is taken forward to Decision 5 and Stage 6.

Enough material was available to construct a full binary phase diagram in Stage 6. Without being particularly

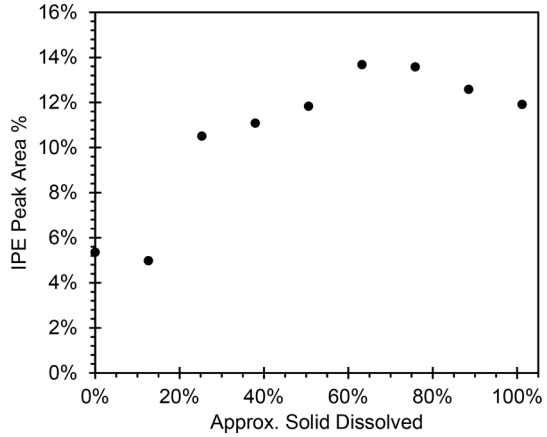

Figure 8. Plot showing the levels of impurity E through the bulk fenofibrate crystalline material.

conservative with material; approximately 250 mg of pure IPE were used to generate the binary phase diagram. The ideal binary phase diagram (see Supporting Information) predicts a eutectic composition of X_{IPE} = 0.629 and a melting temperature of 51.3 °C (Figure 9); however, crystals obtained

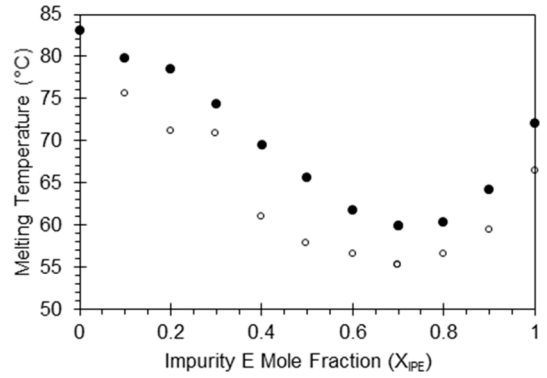

Figure 9. Experimental binary phase diagram of fenofibrate-impurity E system. No eutectic was detected in any sample. (●) Melting peak maxima shown with the corresponding (○) peak onset.

through isothermal evaporation of solution mixtures showed no eutectic signals in any DSC analyses. Consequently, a Tammann triangle cannot be constructed for the FEN−IPE binary system.

By combining this lack of eutectic formation, with the significant impurity concentration after crystallization and the poor purification by reslurry in Stage 3, it was concluded that fenofibrate and impurity E are fully miscible in the solid state,

https://dx.doi.org/10.1021/acs.oprd.0c00166
Org. Process Res. Dev. 2020, 24, 1443−1456

forming a complete solid solution during crystallization. The outcome of Decision 6 in the case of FEN and IPE is therefore "yes". The overall outcome of the workflow for this case study is to change the crude stream composition to decrease the concentration of IPE during crystallization. It is recommended that the synthetic pathway should eliminate the production of impurity E completely, as any amount present is likely to be incorporated into the crystalline material in significant concentrations due to solid solution formation.

Example 3: Paracetamol–Acetanilide. Acetanilide, the *des*-hydroxyl analogue of paracetamol, is metabolized to aniline and is considered a genotoxic impurity.[54] Concentrations in crystal products must be as low as possible. The product specification in this work was 99.8 mol % crystal product purity. The crystallization conditions used allow a maximum possible yield of 67.0%, which leads to a maximum value for α of 0.014.

It has been previously demonstrated that effective purging of ACE can be achieved using a cooling crystallization from 3-methyl-1-butanol,[13] and this was also observed here in 2-propanol. The initial acetanilide concentration c_{ACE} decreased significantly from 5.01 mol % to 0.80 mol % (Table 2, entry 3). The subsequent value for α_{ACE} of 0.063, while reasonably low, is significantly higher than the allowed value, so the material is taken forward to Stage 3. Optical microscopy images of the isolated material are shown in Figure 7b. The image shows free-flowing crystals which are relatively uniform in size and shape, and therefore agglomeration is not the impurity incorporation mechanism. Suspension of crystals in 2-propanol saturated with PCM for 18 h decreased the concentration of ACE from 0.80 mol % to 0.27 mol % (Table 3, entry 2). This is a significant decrease of 66% of c_{ACE}, which gives a positive outcome to Decision 3. Adhesion of ACE to the surface of the PCM crystals was therefore identified as the incorporation mechanism, and it is suggested that modification of the isolation procedure to avoid mother liquor deposits should provide improved PCM purity after crystallization. Indeed, a recent study showed that a stepwise increase of the heptane content while washing PCM crystallized in the presence of ACE leads to enhanced product purity through efficient removal of the impurity from the crystal surface.[55] Another possibility is that small particles of ACE crystallized as a conglomerate toward the end of the initial process, which now redissolve during the reslurry. This is unlikely, as the solubility of ACE is much greater than PCM in 2-propanol.[13]

Example 4: Paracetamol–Metacetamol. Metacetamol is a structural isomer of paracetamol, and while it has antipyretic properties, it is not marketed as a medication. It is not a paracetamol process related impurity, and was chosen here as a model substrate due its almost identical structure to the crystallization target. Using the same conditions as those for the crystallization in the presence of acetanilide, a purity specification of 99.5 mol % increased the allowed α limit to 0.042.

In concurrence with literature, metacetamol is not purged to the same extent as acetanilide during a cooling crystallization of paracetamol.[13,44] The impurity concentration c_{MET} decreased moderately from 4.02 mol % to 2.51 mol % (Table 2, entry 4). The calculated value for α_{MET} (0.251) is almost 6 times larger than the maximum allowed value and is consistent with the previously reported value of 0.250 for similar unseeded cooling crystallizations from 2-propanol.[44] This selectivity coefficient is too high to indicate good impurity rejection, and therefore the crystallized material is taken forward to Stage 3. The microscopy image in Figure 7b shows similar results to ACE. The crystals are not agglomerated, so this is not the mechanism of MET incorporation to PCM. The slurry of crystals in 2-propanol saturated with paracetamol decreased c_{MET} by around 45%, leaving more than half the initial amount of MET in the solid phase (Table 3, entry 3). A meager reduction of c_{MET} from 2.51 mol % to 1.17 mol % is more suggestive of incorporation than surface deposition. Perhaps something akin to the solid solution formation between FEN and IPE. It is hence hypothesized at this stage that a large part of MET is present in crystallized layers inaccessible to the solution during surface washing, and this example is taken forward to Stage 5.

Initial stirring of the suspension resulted in some of the MET dissolving into the liquid phase, in corroboration with the surface washing experiments in Stage 4; a significant amount of the MET must be at the PCM crystal surface. As the overall solid mass dissolves, the MET HPLC peak area of solution increases until complete dissolution is achieved (Figure 10). This confirms that MET is incorporated into the crystal during the growth phase.

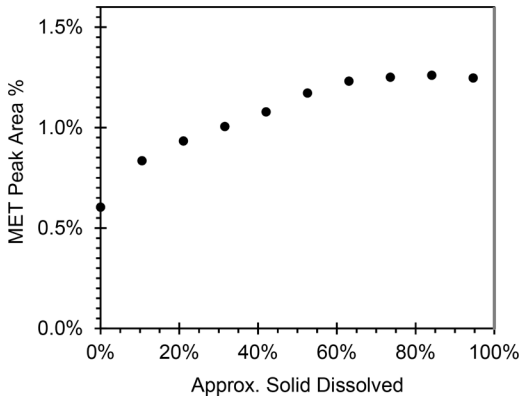

Figure 10. Plot showing the levels of MET through the bulk PCM crystalline material.

In order to carry out Stage 6, crystalline samples of different PCM–MET mole fractions were prepared and analyzed by DSC, and the melting points of the mixtures and eutectics were plotted, along with the predicted relationship (gray lines), to give the binary phase diagram shown in Figure 11a. Plotting the enthalpy associated with eutectic signals (peak area) from the same DSC results against the mole fraction gives the corresponding Tammann triangle (Figure 11b).

The experimental depression in melting point with increasing impurity incorporation matches well the ideal behavior, as does the position of the eutectic. The average eutectic melting temperature was found to be 120.7 ± 1.4 °C, a small deviation from the predicted value of 118.6 °C (see Figure S10). Good linear agreement is also observed in both halves of the Tammann triangle, which give a eutectic composition of X_{MET} = 0.620. The aim of constructing Figure 11b was to look for any miscibility, and indeed, partial miscibility of 6.3 ± 2.3% MET with the PCM is indicated by the left-hand linear regression. While the absolute value is not precise given the associated error, it can be concluded that it is a nonzero value, and therefore MET will be present in the crystalline phase. It can also be seen in Figure 11b that PCM is considered not miscible with the MET, as the *x*-axis intercept

https://dx.doi.org/10.1021/acs.oprd.0c00166
Org. Process Res. Dev. 2020, 24, 1443–1456

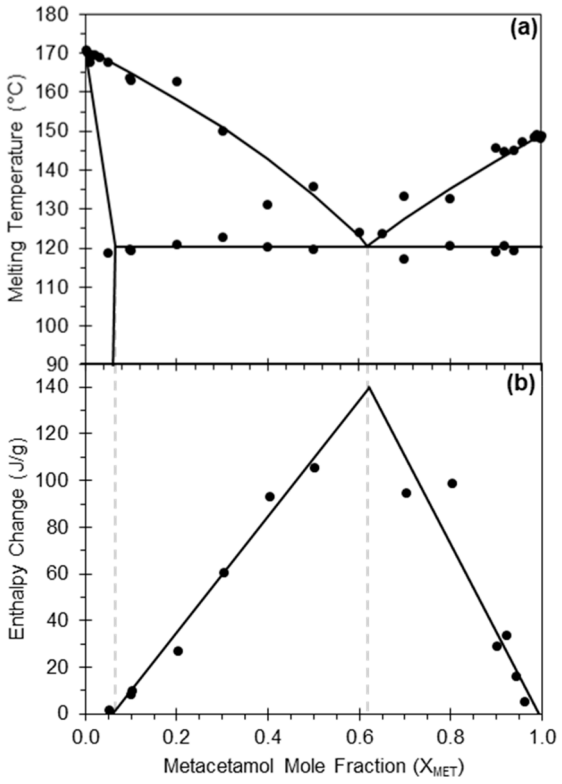

Figure 11. (a) Binary phase diagram for paracetamol-metacetamol, with an average experimental eutectic temperature at 120.7 ± 1.4 °C. (b) Tammann triangle for paracetamol−metacetamol. Left hand side linear regression $y = 249.6x - 15.0$, $R^2 = 0.985$, x-axis intercept = 0.063 ± 0.023. Right hand side linear regression $y = -374.6x + 372.3$, $R^2 = 0.867$, x-axis intercept = 0.977 ± 0.037. Intersection X_{MET} = 0.620, Enthalpy = 139.8 J/g.

of the right-hand linear regression corresponds to a composition of 97.7 ± 3.7%. It can be inferred that paracetamol would be efficiently purged during a crystallization of metacetamol. Combining these two values for miscibility introduces tie-lines to the binary phase diagram, indicated by dashed lines in Figure 11a. The outcome of Decision 6 in the case of paracetamol−metacetamol is therefore "yes", and this leads to the suggestion of changing chemistry to avoid high impurity concentrations in the crude stream to crystallization. During the crystallization, MET is incorporated into the growing PCM crystal through partial miscibility and will be very difficult to remove through a single cooling crystallization.

DISCUSSION

The source of impurity contamination in four representative examples of crystallized APIs has been examined using the workflow methodology depicted in Figure 2, all of which resulted in different outcomes (Table 4). Baseline knowledge (Stage 1) and crystallization (Stage 2) phases of the workflow were straightforward in the discussed examples, as they are well-studied model systems. Comparison of the various selectivity coefficients determined exemplified the difference between good and poor impurity rejection. Fenofibrate can be purified by cooling crystallization from 2-propanol in the presence of substantial initial concentrations of fenofibric acid (α_{FFA} = 0.044); however, this is more challenging in the case of impurity E (α_{IPE} = 0.415).

Table 4. Identified Impurity Inclusion Mechanisms in the Case Studies, and at Which Experimental Stage This Was Identified

Case Study	API	Impurity	Inclusion Mechanism	Stage Identified
1	FEN	FFA	No significant inclusion	2
2	FEN	IPE	Solid solution formation	6
3	PCM	ACE	Surface deposition	3
4	PCM	MET	Partial solid miscibility	6

The optical microscopy images of the isolated samples in Stage 3 ruled out agglomeration as the impurity inclusion method for the three examples which required improved crystal purity. The surface washing experiments completed in Stage 4 effectively discriminated between ACE, as a kinetic impurity deposited on the crystal surface, and IPE and MET, which are thermodynamically incorporated into the growing crystal.

Stage 5 confirmed that both IPE and MET were incorporated throughout the bulk crystal phase. Stepwise dissolution is a destructive technique; however, the valuable knowledge gained through this experiment informs the user that simple modification of process or isolation conditions will not significantly improve the purification efficiency of the crystallization. The binary phase diagrams constructed in Stage 6 revealed different behavior between the IPE-FEN and MET-PCM systems. There was good agreement between ideal behavior and experimental data collected for MET-PCM, and subsequent analysis of the eutectic signals indicated partial miscibility which makes the isolation of paracetamol as a pure component challenging. In contrast, the experimental binary phase diagram IPE-FEN, which deviated significantly from the calculated ideal behavior, showed these two components are fully miscible in the solid state, forming a solid solution. The combination of these case studies demonstrates that by using the workflow methodology, different impurity inclusion mechanisms can be identified.

As this workflow applies to solution crystallization and is, in principle, not limited to pharmaceuticals, the workflow is easily adaptable to other areas of chemical processing and manufacture, such as in food and agrochemical industries.

CONCLUSION

A workflow has been developed which allows users to identify which impurity incorporation mechanism is responsible for a compromised crystalline product purity following a crystallization. This is supported by four pharmaceutical examples with varied impurity inclusion behavior, demonstrating the value of the workflow for successful discrimination between kinetic and thermodynamic mechanisms of impurity inclusion. The experiments that form this workflow are highly informative, but do not necessarily require particularly specialist knowledge or bespoke techniques. They can be carried out using instrumentation available in most chemical laboratories, and therefore the methodology is transferrable to a wide range of applications. While the application of this work to novel multicomponent systems is underway with our hands, we invite other researchers to apply the workflow methodology to their own crystallization development to enhance product purity.

https://dx.doi.org/10.1021/acs.oprd.0c00166
Org. Process Res. Dev. 2020, 24, 1443−1456

MATERIALS AND METHODS

Paracetamol (≥99.0%, Sigma-Aldrich), acetanilide (99%, Sigma-Aldrich), metacetamol (97%, Sigma-Aldrich), and fenofibrate (≥99%, Sigma-Aldrich) were purchased and used without further purification.[56] Fenofibric acid and ethyl 2-[4-(4-chlorobenzoyl)phenoxy]-2-methylpropanoate (fenofibrate EP impurity E) were synthesized using literature procedures,[56] and their purities were confirmed by ^{1}H NMR spectroscopy, HPLC, and DSC analysis. Solvents 2-propanol (99.7%, VWR International), heptane (99%, Sigma-Aldrich), methanol (HPLC grade, 99.9%, Sigma-Aldrich), acetonitrile (HPLC grade, 99.9%, VWR International), acetone (99.8%, VWR International), and ethanol (99.8%, VWR International) were purchased and used without further purification.

Crystallization. Small scale batch crystallizations were carried out using the Technobis Crystalline, which consists of a metal jacket for temperature control and inline turbidity measurement. An amount of API was weighed into an 8 mL vial containing a magnetic stirrer bar, followed by an amount of impurity. 2-Propanol was added to give 4 mL suspensions of known API and impurity concentration (paracetamol 310 mg g^{-1}, fenofibrate 145 mg g^{-1}). The stirred vials were then heated above the suspension saturation temperature, held briefly isothermally to ensure complete dissolution, and then cooled rapidly (5 °C min^{-1}) to the temperature to reach the desired relative supersaturation ratio S, as defined by eq 3 where x is the concentration (mg g^{-1}) of the solution and x^* is the saturation concentration (mg g^{-1}) of the system at that temperature. The solution was held isothermally at this temperature for 30 min, during which time nucleation occurred, indicated by a sudden decrease in transmissivity, and the formation of a suspension was confirmed by analysis of in situ images. The nucleated suspension was cooled slowly (0.5 °C min^{-1}) to 15 °C and finally held at this final temperature for an extended time (1.5 h for paracetamol, 3.5 h for fenofibrate).

$$S = \frac{x}{x^*} \tag{3}$$

After crystallization, a portion of filtered mother liquor phase was transferred to a preweighed vial, the mass was recorded, and the solvent was evaporated from the sample using an IKA multiwell heat block at 45 °C to give a gravimetric concentration. The evaporated mother liquor sample was diluted directly with mobile phase for high-performance liquid chromatography (HPLC). The remaining suspension from the crystallization was then vacuum filtered, and the solid was washed with heptane (for paracetamol, 2 × 2 mL),[13] or saturated fenofibrate stock solution (fenofibrate, 2 mL). A measured amount of the crystals isolated was diluted with HPLC mobile phase volumetrically to a concentration within the calibrated limits.

Solid State Analysis. HPLC was used to measure component concentrations in the solid and isolated liquid phases after crystallization, surface washing, and reslurry. Calibration curves were constructed to allow accurate concentration determination (Figure S3); however, similar results could be obtained by using relative area%. This latter method could be used if the impurities were not available in their pure form for calibration, or if the identity of the impurities is unknown. HPLC analysis was carried out using an Agilent 1100 instrument fitted with an Agilent Poroshell 120, EC-C18, 4.6 mm × 74 mm 2.7 μm column. For paracetamol samples, solids were dissolved in 5% MeOH in H_2O and a mobile phase of 20% MeOH in H_2O was used. An isocratic elution of 1 mL min^{-1} was used, at a column temperature of 40 °C. The analysis was stopped after 12 min. For fenofibrate samples, solids were dissolved in MeCN, and a mobile phase of 20% acidified H_2O (pH = 3, acidified with H_3PO_4) in MeCN was used. An isocratic elution of 1 mL min^{-1} was used, at a column temperature of 25 °C. The analysis was stopped after 15 min, and between each sample an MeCN "blank" sample was passed through the column under the same conditions. The resulting chromatographs were analyzed using the Agilent ChemStation software.

The polymorphic form of the API crystallized was analyzed using a Bruker AXS D8 Advance II diffractometer using Debye−Scherrer transmission of Cu Kα1 radiation with a wavelength of 1.540596 Å. Samples were prepared on an automated x-y 28 well plate with 7.5 μm Kaptopn film. Patterns were collected in the range 4−35 2θ and were compared to reference patterns located in the Cambridge Crystallographic Data Centre (CCDC) to identify the polymorph present.

Images were captured using a Leica DM6000 FS microscope. Small amounts of crystals were transferred to microscope slides and viewed with an appropriate magnification to identify any agglomeration.

Differential Scanning Calorimetry (DSC) measurements were carried out using a Netzsch DSC214 Polyma. Experimental conditions used were based on literature reported DSC studies of paracetamol and fenofibrate, and a single heating−cooling cycle was used to avoid polymorphic transformations.[57,58] Samples were heated at a rate of 10 °C min^{-1} to 10 °C higher than the melting temperatures of the pure components, held isothermally for 10 min, and then returned to room temperature at a rate of 10 °C min^{-1}.

Using the literature reported values for the solubility of paracetamol, metacetamol, and acetanilide in acetone,[59] volumetric stock solutions of each solute with the same molar concentration were prepared. These solutions were then combined in different binary ratios to give solutions of different impurity mole fractions X_i. These solutions were evaporated at room temperature to give crystalline material suitable for DSC analysis. The melting temperature of the component and eutectic signals were plotted as a function of X_i to give the experimental binary phase diagram. A similar procedure was followed for fenofibrate using ethanol solutions, as impurity E was found to have insufficient solubility in acetone.

Where evaporation of the solvent gave a crystalline solid suitable for thermal analysis, the solid was subjected to DSC analysis. Typically, the resulting DSC graph contained two signals, one corresponding to the component melting enthalpy and the other corresponding to the eutectic melting enthalpy. Typically, the component melting temperature changes significantly with solid composition, where the eutectic melting temperature does not. For the binary phase diagram, the melting peak maxima of both signals were plotted as a function of mole fraction composition. Where the DSC graphs contained a eutectic peak, the integrated area of this signal was plotted as a function of the impurity mole fraction X_i in the solid phase to give the Tammann plot. A linear fit of these data points gives two linear relationships which intersect at a maximum energy value, with a X_i value corresponding to the eutectic composition.[51] The miscibility limit of the solid−solid

https://dx.doi.org/10.1021/acs.oprd.0c00166
Org. Process Res. Dev. 2020, 24, 1443−1456

composition is determined by the linear extrapolation to the intersection of the X_i-axis.

Stepwise Dissolution. An amount of solid isolated from the crystallization was suspended in a saturated API solution, with a solid loading of approximately 100 mg mL^{-1}, and was stirred for at least 30 min. A filtered sample was removed (0.01 to 0.02 mL, depending on system), the mass was recorded, and the solution was diluted directly for HPLC analysis. Portions of pure solvent were then added to the suspension, calculated from solubility curves to dissolve approximately 10 w% of the material with each addition, and the suspension stirred for a further 10−15 min, before another sample was taken and diluted directly for HPLC analysis. This process was repeated until the crystals were completely dissolved. The concentrations of the API and impurity were determined by HPLC analysis.

■ ASSOCIATED CONTENT

Supporting Information

The Supporting Information is available free of charge at https://pubs.acs.org/doi/10.1021/acs.oprd.0c00166.

Further detailed experimental details for each of the case studies, including analytical and characterization data for crystallization products (PDF)

■ AUTHOR INFORMATION

Corresponding Author

Joop H. Ter Horst − *EPSRC Centre for Innovative Manufacturing in Continuous Manufacturing and Crystallisation, University of Strathclyde, Glasgow G1 1RD, U.K.*; orcid.org/0000-0003-0118-2160; Email: joop.terhorst@strath.ac.uk

Authors

Stephanie J. Urwin − *EPSRC Centre for Innovative Manufacturing in Continuous Manufacturing and Crystallisation, University of Strathclyde, Glasgow G1 1RD, U.K.*; orcid.org/0000-0002-9092-0200

Guillaume Levilain − *Bayer AG, Forschungszentrum Aprath, 42096 Wuppertal, Germany*

Ivan Marziano − *Pfizer Worldwide Research and Development, Sandwich CT13 9NJ, U.K.*

Jeremy M. Merritt − *Eli Lilly and Company, Small Molecule Design and Development, Lilly Technology Center North, Indianapolis, Indiana 46221, United States*

Ian Houson − *EPSRC Centre for Innovative Manufacturing in Continuous Manufacturing and Crystallisation, University of Strathclyde, Glasgow G1 1RD, U.K.*

Complete contact information is available at: https://pubs.acs.org/10.1021/acs.oprd.0c00166

Author Contributions

S.J.U. devised and performed experiments and cowrote the manuscript. G.L., I.M., and J.M.M. contributed equally to this publication, steering the project and giving significant industrial perspective. I.H. managed the project and collaborative interactions and gave valuable scientific advice. J.H.t.H. designed and supervised the study and cowrote the manuscript.

Notes

The authors declare no competing financial interest.

■ ACKNOWLEDGMENTS

The authors would like to thank EPSRC, Centre for Innovative Manufacturing in Continuous Manufacturing and Crystallization (CMAC) (Grant ref EP/I033459/1) and the CMAC Tier 1 companies GlaxoSmithKline, AstraZeneca, Novartis, Bayer AG, Eli Lilly and Company, Takeda, Roche and Pfizer for funding and supporting this work. We specifically acknowledge the Technical Committee for helpful discussions and constructive feedback on the workflow. The authors would also like to acknowledge that this work was carried out in the CMAC National Facility, housed within the University of Strathclyde's Technology and Innovation Centre, and funded with a UKRPIF (UK Research Partnership Institute Fund) capital award, SFC ref H13054, from the Higher Education Funding Council for England (HEFCE). The authors thank Dr. Stephanie Yerdelen for her experimental help and stimulating discussions.

■ REFERENCES

(1) ter Horst, J. H.; Schmidt, C.; Ulrich, J. Fundamentals of Industrial Crystallization. In *Handbook of Crystal Growth*; Elsevier B.V., 2015; pp 1317−1349. DOI: 10.1016/B978-0-444-63303-3.00032-8.

(2) Statement alerting patients and health care professionals of NDMA found in samples of ranitidine https://www.fda.gov/news-events/press-announcements/statement-alerting-patients-and-health-care-professionals-ndma-found-samples-ranitidine.

(3) Laboratory Analysis of Ranitidine and Nizatidine Products https://www.fda.gov/drugs/drug-safety-and-availability/laboratory-tests-ranitidine.

(4) Görög, S. The Importance and the Challenges of Impurity Profiling in Modern Pharmaceutical Analysis. *TrAC, Trends Anal. Chem.* **2006**, *25* (8), 755−757.

(5) Cheng, Y. S.; Lam, K. W.; Ng, K. M.; Wibowo, C. Workflow for Managing Impurities in an Integrated Crystallisation Process. *AIChE J.* **2009**, *56* (3), 633−649.

(6) Moynihan, H. A.; Horgan, D. E. Impurity Occurrence and Removal in Crystalline Products from Process Reactions. *Org. Process Res. Dev.* **2017**, *21*, 689−704.

(7) Darmali, C.; Mansouri, S.; Yazdanpanah, N.; Woo, M. W. Mechanisms and Control of Impurities in Continuous Crystallization: A Review. *Ind. Eng. Chem. Res.* **2019**, *58*, 1463−1479.

(8) Lorenz, H.; Beckmann, W. Purification by Crystallization. *Cryst. Basic Concepts Ind. Appl.* **2013**, 129−148.

(9) Pietsch, W. Undesired Agglomeration: Methods of Avoiding or Lessening Its Effect. In *Agglomeration in Industry: Occurence and Applications*; WILEY-VCH Verlag GmbH & Co.: 2004. DOI: 10.1002/9783527619795.

(10) Mullin, J. W. *Crystallization*; Butterworth-Heinemann: Oxford, 2001.

(11) Ålander, E. M.; Uusi-Penttilä, M. S.; Rasmuson, Å. C. Agglomeration of Paracetamol during Crystallization in Pure and Mixed Solvents. *Ind. Eng. Chem. Res.* **2004**, *43* (2), 629−637.

(12) Gielen, B.; Jordens, J.; Thomassen, L. C. J.; Braeken, L. *Crystals* **2017**, *7*, 40.

(13) Nguyen, T.; Khan, A.; Bruce, L.; Forbes, C.; O'Leary, R.; Price, C. The Effect of Ultrasound on the Crystallisation of Paracetamol in the Presence of Structurally Similar Impurities. *Crystals* **2017**, *7*, 294−318.

(14) Simone, E.; Othman, R.; Vladisavljević, G. T.; Nagy, Z. K. Preventing Crystal Agglomeration of Pharmaceutical Crystals Using Temperature Cycling and a Novel Membrane Crystallization Procedure for Seed Crystal Generation. *Pharmaceutics* **2018** *10* (1). 17.

(15) Fiebig, A.; Jones, M. J.; Ulrich, J. Predicting the Effect of Impurity Adsorption on Crystal Morphology. *Cryst. Growth Des.* **2007**, *7* (9), 1623−1627.

(16) Davey, R. J. The Effect of Impurity of Adsorption on the Kinetics of Crystal Growth from Solution. *J. Cryst. Growth* **1976**, *34*, 109−119.
(17) Kubota, N. Effect of Impurities on the Growth Kinetics of Crystals. *Cryst. Res. Technol.* **2001**, *36* (8−10), 749−769.
(18) Hayes, J. A.; Eccles, K. S.; Lawrence, S. E.; Moynihan, H. A. Methyl Tetra-O-Acetyl-α- D -Glucopyranuronate: Crystal Structure and Influence on the Crystallisation of the β Anomer. *Carbohydr. Res.* **2016**, *425*, 35−39.
(19) Yan, S.; Xie, C.; Zhang, X.; Zhou, L.; Hou, B.; Huang, J.; Zhou, L.; Yin, Q. Influence of Crystal Growth Conditions on Formation of Macroscopic Inclusions inside Thiourea Crystals. *ChemistrySelect* **2018**, *3* (8), 2293−2297.
(20) Meadhra, R.; Kramer, H. J. M.; Van Rosmalen, G. M. Model for Secondary Nucleation in a Suspension Crystallizer. *AIChE J.* **1996**, *42* (4), 973−982.
(21) Gu, C. H.; Grant, D. J. W. Relationship between Particle Size and Impurity Incorporation during Crystallization of (+)-Pseudoephedrine Hydrochloride, Acetaminophen, and Adipic Acid from Aqueous Solution. *Pharm. Res.* **2002**, *19* (7), 1068−1070.
(22) Chow, A. H. L.; Chow, P. K. K.; Zhongshan, W.; Grant, D. J. W. Modification of Acetaminophen Crystals: Influence of Growth in Aqueous Solutions Containing P-Acetoxyacetanilide on Crystal Properties. *Int. J. Pharm.* **1985**, *24* (2−3), 239−258.
(23) Ukrainczyk, M.; Hodnett, B. K.; Rasmuson, Å. C. Process Parameters in the Purification of Curcumin by Cooling Crystallization. *Org. Process Res. Dev.* **2016**, *20* (9), 1593−1602.
(24) Givand, J. C.; Teja, A. S.; Rousseau, R. W. Manipulating Crystallization Variables to Enhance Crystal Purity. *J. Cryst. Growth* **1999**, *198-199*, 1340−1344.
(25) Duggirala, N. K.; Perry, M. L.; Almarsson, Ö.; Zaworotko, M. J. Pharmaceutical Cocrystals: Along the Path to Improved Medicines. *Chem. Commun.* **2016**, *52* (4), 640−655.
(26) Karimi-Jafari, M.; Padrela, L.; Walker, G. M.; Croker, D. M. Creating Cocrystals: A Review of Pharmaceutical Cocrystal Preparation Routes and Applications. *Cryst. Growth Des.* **2018**, *18* (10), 6370−6387.
(27) Karagianni, A.; Malamatari, M. Pharmaceutical Cocrystals: New Solid Phase Modification Approaches for the Formulation of APIs. *Pharmaceutics* **2018**, *10*, 18.
(28) Ranganathan, A.; Pedireddi, V. R.; Rao, C. N. R. Hydrothermal Synthesis of Organic Channel Structures: 1:1 Hydrogen-Bonded Adducts of Melamine with Cyanuric and Trithiocyanuric Acids. *J. Am. Chem. Soc.* **1999**, *121*, 1752−1753.
(29) Florence, A. J.; Leech, C. K.; Shankland, N.; Shankland, K.; Johnston, A. Control and Prediction of Packing Motifs: A Rare Occurrence of Carbamazepine in a Catemeric Configuration. *CrystEngComm* **2006**, *8* (10), 746−747.
(30) Cruz Cabeza, A. J.; Day, G. M.; Motherwell, W. D. S.; Jones, W. Solvent Inclusion in Form II Carbamazepine. *Chem. Commun.* **2007**, *12* (16), 1600−1602.
(31) Fabbiani, F. P. A.; Byrne, L. T.; McKinnon, J. J.; Spackman, M. A. Solvent Inclusion in the Structural Voids of Form II Carbamazepine: Single-Crystal X-Ray Diffraction, NMR Spectroscopy and Hirshfeld Surface Analysis. *CrystEngComm* **2007**, *9* (9), 728−731.
(32) Case, D. H.; Srirambhatla, V. K.; Guo, R.; Watson, R. E.; Price, L. S.; Polyzois, H.; Cockcroft, J. K.; Florence, A. J.; Tocher, D. A.; Price, S. L. Successful Computationally Directed Templating of Metastable Pharmaceutical Polymorphs. *Cryst. Growth Des.* **2018**, *18* (9), 5322−5331.
(33) Horgan, D. E.; Crowley, L. M.; Stokes, S. P.; Lawrence, S. E.; Moynihan, H. A. Impurity Exclusion and Retention during Crystallisation and Recrystallisation — The Phenacetin by Ethylation of Paracetamol Process. *Advanced Topics in Crystallization* **2015**, 57−84.
(34) Burel, A.; Couvrat, N.; Tisse, S.; Cartigny, Y.; Cardinael, P.; Coquerel, G. Binary Phase Diagrams between Phenanthrene and Two of Its Impurities: 9,10-Dihydroanthracene and Carbazole. *Eur. Phys. J.: Spec. Top.* **2017**, *226* (5), 869−880.
(35) Beckmann, W.; Lorenz, H. Partial Miscibility of Organic Compounds in the Solid State - The Case of Two Epimers of a Diastereoisomer. *Chem. Eng. Technol.* **2006**, *29*, 226−232.
(36) Brown, C. J.; McGlone, T.; Yerdelen, S.; Srirambhatla, V.; Mabbott, F.; Gurung, R.; Briuglia, M. L.; Ahmed, B.; Polyzois, H.; McGinty, J.; Perciballi, F.; Fysikopoulos, D.; MacFhionnghaile, P.; Siddique, H.; Raval, V.; Harrington, T. S.; Vassileiou, A. D.; Robertson, M.; Prasad, E.; Johnston, A.; Johnston, B.; Nordon, A.; Srai, J. S.; Halbert, G.; ter Horst, J. H.; Price, C. J.; Rielly, C. D.; Sefcik, J.; Florence, A. J. Enabling Precision Manufacturing of Active Pharmaceutical Ingredients: Workflow for Seeded Cooling Continuous Crystallisations. *Mol. Syst. Des. Eng.* **2018**, *3*, 518−549.
(37) International Conference on Harmonisation of Technical Requirements for Registration of Pharmaceuticals from Human Use: Impurities in New Drug Products (Q3B(R2)), 2006.
(38) Qian, G.; Wu, Y.; Yang, X.; Zhou, X. Exploiting Polymorphism in the Purity Enhancement of Lincomycin Hydrochloride. *Chem. Eng. Sci.* **2012**, *77*, 42−46.
(39) Simone, E.; Steele, G.; Nagy, Z. K. Tailoring Crystal Shape and Polymorphism Using Combinations of Solvents and a Structurally Related Additive. *CrystEngComm* **2015**, *17* (48), 9370−9379.
(40) Black, S. N.; Cuthbert, M. W.; Roberts, R. J.; Stensland, B. Increased Chemical Purity Using a Hydrate. *Cryst. Growth Des.* **2004**, *4* (3), 539−544.
(41) Holm, R.; Elder, D. P. Analytical Advances in Pharmaceutical Impurity Profiling. *Eur. J. Pharm. Sci.* **2016**, *87*, 118−135.
(42) Abramov, Y. A. Rational Solvent Selection for Pharmaceutical Impurity Purge. *Cryst. Growth Des.* **2018**, *18* (2), 1208−1214.
(43) Caspi, D. D.; Nordstrom, F. L. Quantitative Impurity Rejection Analysis for Crystallization. *Org. Process Res. Dev.* **2018**, *22* (7), 856−861.
(44) Hendriksen, B. A.; Grant, D. J. W.; Meenan, P.; Green, D. A. Crystallisation of Paracetamol (Acetaminophen) in the Presence of Structurally Related Substances. *J. Cryst. Growth* **1998**, *183*, 629−640.
(45) Pitt, K.; Peña, R.; Tew, J. D.; Pal, K.; Smith, R.; Nagy, Z. K.; Litster, J. D. Particle Design via Spherical Agglomeration: A Critical Review of Controlling Parameters, Rate Processes and Modelling. *Powder Technol.* **2018**, *326*, 327−343.
(46) Moynihan, H. A.; Armstrong, D. Determination of Composition Distributions of Multi-Particle Crystalline Samples by Sequential Dissolution with Concomitant Particle Sizing and Solution Analysis. *CrystEngComm* **2018**, *20*, 2617−2633.
(47) Moynihan, H. A.; Armstrong, D. Stepwise Dissolution and Composition Determination of Samples of Multiple Crystals Using and Fluorocarbon Phases. *RSC Adv.* **2019**, *9*, 21405−21417.
(48) Teerakapibal, R.; Li, H.; Linehan, B.; Nordstrom, F. L. Material Impurity Distribution of Lattice-Incorporated Impurities in Salicylic Acid. *Cryst. Growth Des.* **2020**, *20* (3), 1716−1728.
(49) Waldschmidt, A.; Dupray, V.; Berton, B.; Couvrat, N.; Petit, S.; Coquerel, G. Incidence of Crystal Growth Conditions on the Formation of Macroscopic Liquid Inclusions in Ciclopirox Crystals. *J. Cryst. Growth* **2012**, *342* (1), 72−79.
(50) Wang, Y.; Zhang, N.; Hou, B.; Yin, Q.; Gong, J.; Tang, W. Effect of Crystal Growth Kinetics on the Formation of Liquid Inclusions in Tetramethylpyrazine Crystals. *CrystEngComm* **2020**, *22* (11), 1991−2001.
(51) Rycerz, L. Practical Remarks Concerning Phase Diagrams Determination on the Basis of Differential Scanning Calorimetry Measurements. *J. Therm. Anal. Calorim.* **2013**, *113*, 231−238.
(52) Corvis, Y.; Menet, M. C.; Espeau, P. Incidence of the Melting-Degradation Process of Vitamin C on the Determination of the Phase Diagram with Acetaminophen Enhanced by High Performance Liquid Chromatography Tools. *New J. Chem.* **2015**, *39*, 1938−1942.
(53) Leitner, J.; Jurik, S. DSC Study and Thermodynamic Modelling of the System Paracetamol−o-Acetylsalicylic Acid. *J. Therm. Anal. Calorim.* **2017**, *130*, 1735−1740.
(54) Brodie, B. B.; Axelrod, J. The Fate of Acetanilide in Man. *J. Pharmacol. Experiemental Ther.* **1948**, 29−38.

https://dx.doi.org/10.1021/acs.oprd.0c00166
Org. Process Res. Dev. 2020, 24, 1443−1456

(55) Shahid, M.; Sanxaridou, G.; Ottoboni, S.; Lue, L.; Price, C. Understanding and Mitigating the Consequences of Undesired Crystallisation Taking Place during Washing of Active Pharmaceuticals. In *British Association of Crystal Growth 50th Annual Conference*, London, United Kingdom, 2019.
(56) Patil, R.; Patil, S.; Joshi, P.; Jadhav, V. Synthesis and Characterization of Potential Impurities in Fenofibrate Drug Substance. *Der Pharma Chem.* **2015**, *7*, 273−278.
(57) Heinz, A.; Gordon, K. C.; Mcgoverin, C. M.; Rades, T.; Strachan, C. J. Understanding the Solid-State Forms of Fenofibrate − A Spectroscopic and Computational Study. *Eur. J. Pharm. Biopharm.* **2009**, *71* (1), 100−108.
(58) De Wet, F. N.; Gerber, J. J.; Lötter, A. P.; Van der Watt, J. G.; Dekker, T. G. A Study of the Changes during Heating of Paracetamol. *Drug Dev. Ind. Pharm.* **1998**, *24* (5), 447−453.
(59) Granberg, R. A.; Rasmuson, Å. C. Solubility of Paracetamol in Pure Solvents. *J. Chem. Eng. Data* **1999**, *44*, 1391−1395.

https://dx.doi.org/10.1021/acs.oprd.0c00166
Org. Process Res. Dev. 2020, 24, 1443−1456